View metadata, citation and similar papers at core.ac.uk
brought to you by CORE
provided by Archive Ouverte en Sciences de l'Information et de la Communication

VACANCY-MEDIATED ATOMIC TRANSPORT IN NANO-CRYSTALS

A. Portavoce, J Perrin-Toinin, K. Hoummada

▶ To cite this version:

A. Portavoce, J Perrin-Toinin, K. Hoummada. VACANCY-MEDIATED ATOMIC TRANSPORT IN NANO-CRYSTALS. Reviews on Advanced Materials Science, 2016. hal-02385245

HAL Id: hal-02385245
https://hal-amu.archives-ouvertes.fr/hal-02385245

Submitted on 28 Nov 2019

HAL is a multi-disciplinary open access archive for the deposit and dissemination of scientific research documents, whether they are published or not. The documents may come from teaching and research institutions in France or abroad, or from public or private research centers.

L'archive ouverte pluridisciplinaire **HAL**, est destinée au dépôt et à la diffusion de documents scientifiques de niveau recherche, publiés ou non, émanant des établissements d'enseignement et de recherche français ou étrangers, des laboratoires publics ou privés.

Rev. Adv. Mater. Sci. 50 (2017) 69-75

VACANCY-MEDIATED ATOMIC TRANSPORT IN NANO-CRYSTALS

A. Portavoce[1], J. Perrin-Toinin[2] and K. Hoummada[2]

[1]CNRS, IM2NP, Faculté des Sciences et Techniques de Saint-Jérôme case 142, 13397 Marseille, France
[2]Aix-Marseille University, IM2NP, Faculté des Sciences et Techniques de Saint-Jérôme case 142, 13397 Marseille, France

Received: March 10, 2016

Abstract. Atomic transport in nano-crystals is still poorly studied experimentally. However, the knowledge of atomic transport kinetic and of the mechanisms allowing atoms to move in a volume exhibiting nano-scale dimensions (< 100 nm) is important for i) improving our fundamental knowledge concerning point defects' formation and migration energies, and atom-point defect interactions in nano-structures, as well as for ii) predicting mass transport in nano-structures, allowing the design of nano-structure fabrication processes to be developed at lower cost. In this article, atom probe tomography measurements were used to investigate the Ge distribution in 40 nm-wide Si nano-crystals in which the Ge flux was found to be ten times faster than in the bulk of a Si mono-crystal. The Ge atoms were found to be randomly distributed in the nano-crystals. No extended defect was found being able to explain an increase of Ge transport kinetic in the nano-crystals. Consequently, a scenario based on a higher equilibrium vacancy concentration at the nano-crystal surface (or interface) is proposed in order to explain the faster atomic kinetic measured in Si nano-crystals.

1. INTRODUCTION

Experimental measurement of atomic transport kinetic allows point-defects' average energies of formation and migration to be measured [1-6], and informs on point-defect concentrations [1-6], as well as on atoms and point-defects [1-6] or extended defects [7-11] interactions. Atomic diffusion experiments were mainly used (with success) to probe bulk material atomic properties [1-5], and only few experimental studies concerning atomic transport in nano-crystals were reported in the literature, allowing atomic properties in nano-materials to be better understood [12-21]. Indeed, atom-atom interactions and atom-defect interactions in nano-objects embedded in the nanostructures used in nanotechnologies are key parameters in order to produce the desired nanostructures and to come up with technological solutions improving their stability (nano-material ageing). Si is the base material used in the microelectronics complementary metal oxide semiconductor (CMOS) technology, and a large number of future applications are expected to use Si-based nanostructures such as nano-crystalline films [22-24], nano-wires [25-27], and nano-dots [28-30]. The study of Ge diffusion in nano-crystalline Si made of 40 nm-wide grains led to the conclusion that Ge atomic transport was faster in a Si nano-crystal than in the bulk of an infinite Si crystal [13,14]. This result is surprising and is still not yet understood. One could note that

Corresponding author: A. Portavoce, e-mail: alain.portavoce@im2np.fr

© 2017 Advanced Study Center Co. Ltd.

the Ge diffusivity in nano-crystals was observed to be the same as in the mono-crystal when the annealing temperature gets closer to the Si melting temperature [18]. Considering that Ge diffusion was shown to be mainly vacancy-mediated in Si [5,6,31,32], this last observation could be interpreted by a higher vacancy concentration in the nano-volume, with a concentration difference between macro- and nano-volumes decreasing when the temperature increases. However, before to look for further reasons explaining a faster atomic transport kinetic in the Si nano-crystals, the possible existence of fast diffusion paths in the nano-crystal need to be ruled out.

In this work, laser-pulsed atom probe tomography (APT) was used to investigate at the atomic scale the Ge distribution in the Si nano-crystalline layers in which the Ge lattice diffusion kinetic was found to be one order of magnitude faster than in Si bulk. Ge was found to be randomly distributed in volumes exhibiting sizes close to the average nano-grain size. The concentration profiles obtained with these Ge random distributions are in agreement with the profiles measured by secondary ion mass spectrometry used to measure the Ge diffusion coefficient, suggesting that Ge atoms used lattice diffusion in the nano-grains, without the use of fast diffusion paths such as dislocations. Thus, we proposed a scenario based on the difference of vacancy concentration between the surfaces (or interfaces) and the bulk of the nanocrystals to explain the faster Ge diffusion observed in Si nano-grains.

2. EXPERIMENTS

The nano-Si layers used in refs. [13] and [14] to measure the Ge diffusion coefficient in Si nano-grains, grain boundaries and triple junctions were analyzed by laser-pulsed atom probe tomography (APT) using a LEAP 3000X HR microscope. The samples were made of a 500 nm-thick nano-crystalline Si layer deposited at low temperature by chemical vapour deposition on a B-doped Si(001) substrate and exhibiting an average grain size of 40 nm [13]. The Ge diffusion source was implanted in the nano-crystalline layer after growth using an energy of 180 keV [13]. The samples were prepared for APT analysis using a Helios NanoLab Dual Beam Ga^+ focused ion beam from FEI, after covering the samples' surface with a 100 nm-thick Ni film by magnetron sputtering for protection [33]. The APT measurements were performed at 20K, with a laser pulse frequency of 100 kHz, using a laser power of 0.5 nJ.

3. RESULTS AND DISCUSSION

Fig. 1 presents APT measurements obtained on the sample annealed at T = 850 °C for one hour [13]. Fig. 1a shows the entire volume (40 × 40 × 350 nm^3), and Fig. 1b presents a 20 nm-thick slice taken in the center of the same volume. Each dot is a single atom, gray dots and red dots corresponding to Si and Ge atoms, respectively. In this figures, only 0.1% of the entire Si atoms are shown, while 100% of the Ge atoms are presented. The lateral size of the region exhibiting the highest Ge concentration in this volume (depth ~ 100 nm) is about the same as the Si nano-grains' average size. The Ge atoms are randomly distributed. This is confirmed by a statistical study presented in Fig. 1c, showing that the Ge distribution in the entire volume (solid line) follows a random binomial distribution (dash line) centered on the average Ge concentration (~ 2 × 10^{-4} %). APT measurements did not evidence any extended defects in which Ge atoms could gather and diffuse faster in the Si nano-grains. In addition, the one-dimensional (1D) composition profiles measured by APT, corresponding to randomly distributed Ge atoms in the nano-crystalline layer, were found to be in good agreement with the secondary ion mass spectrometry (SIMS) profiles measured in the corresponding samples [13], showing that the SIMS profiles were not modified by grain boundary migration [34]. These observations suggest that the Ge atoms diffused in the Si nano-crystals without the use of extended defects such as dislocations, and that the diffusion coefficient measured in the Si nano-grains using the SIMS profiles manly corresponds to Ge vacancy-mediated lattice diffusion [5,6,31,32]. Thus, the understanding of a faster Ge atomic transport in Si nano-crystals is still needed. One can note that the Si(111) surface melting was found to occur at $T_{sm} = 0.84 T_m$ (with T_m the Si bulk melting temperature), which corresponds to a $\Delta T_m = T_m - T_{sm}$ ~ 200 °C [35,36]. Si surface pre-melting confirms that the vacancy concentration at a material surface is in general larger than in the material bulk. For example, in the case of Sb diffusion in monocrystalline Si(Ge), the diffusivity was found to be several orders of magnitude faster in the sub-surface region compared to deeper into the bulk, despite that Sb diffusion was found to be vacancy mediated both in the bulk and under the surface [37,38]. Positron annihilation measurements shown that the concentration of vacancies (V) can vary significantly over tens of nanometers from a maximum at the surface until reaching a lower concentration plateau in the bulk of semiconductors

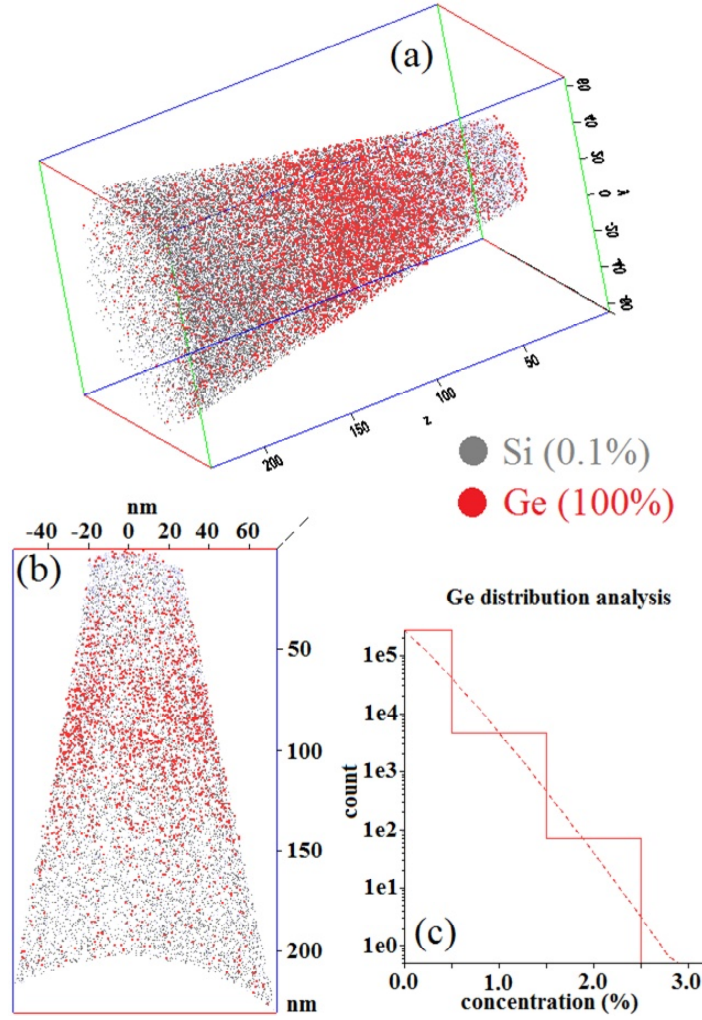

Fig. 1. APT measurements performed on the Ge-implanted Si nanocrystalline layer annealed at 850 °C for one hour: a) an entire APT volume showing 0.1% of the detected Si atoms (gray dots) and 100% of the detected Ge atoms (red dots); b) a 20 nm-thick slice taken in the center of the same volume; and c) the atomic distribution of Ge atoms in the APT volume (solid line) compared to an atomic random distribution (dash line).

[39-40]. For example, it was shown that at 400 °C, a depth of ~ 300 nm is needed to be reached in Si in order to observe a constant vacancy concentration [39]. All these results suggest that, at a given temperature, the vacancy equilibrium concentration at the surface (C_{Vs}^*) is higher than in the bulk (C_V^*), and that a stationary state may be reached between the surface and the bulk at equilibrium, forming a decreasing vacancy concentration gradient from the surface to the bulk on several nanometers deep before to reach a constant value. As a first approximation, one can use the data from the literature giving the Si bulk equilibrium vacancy concentration versus T to determine C_{Vs}^* from C_V^* considering that, for a given annealing temperature T_a, C_{Vs}^* corresponds to the value of C_V^* at $T = T_a + \Delta T_m$. For example, at T_a = 950 °C (in the annealing temperature range used in refs. [13] and [14]) one would obtain $C_V^* = 8 \times 10^{14}$ cm^{-3} and $C_{Vs}^* = 1 \times 10^{16}$ cm^{-3} from ref. [1]. Thus, vacancy diffusion in Si bulk during annealing can be simulated in a simplified way considering the diffusion equation

$$\frac{\mathrm{d}C_V}{\mathrm{d}t} = D_V \frac{\mathrm{d}^2 C_V}{\mathrm{d}x^2} - k\left(C_V - C_V^*\right), \quad (1)$$

with C_V the local vacancy concentration, D_V the vacancy diffusion coefficient, and k the bulk vacancy annihilation/formation rate. During annealing in a diffusion furnace, the sample temperature changes rapidly from room temperature T_0 to T_a, and thus, the vacancy concentration increases from $C_V^*(T_0)$ (which is negligible [1,5]) to $C_V^*(T_a)$. Kinetics being faster at the surface compared to in the bulk, $C_{Vs}^*(T_a)$ could be considered to be reached as soon as T_a is

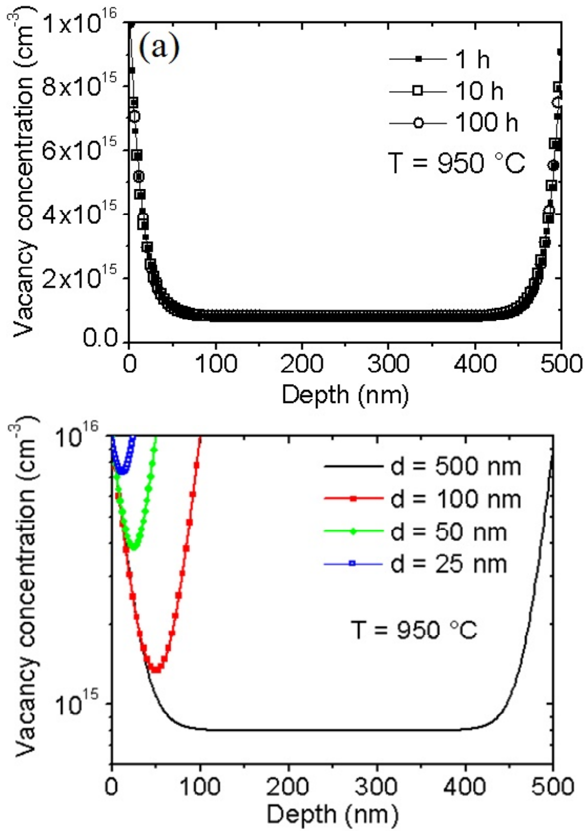

Fig. 2. Vacancy concentration profiles simulated at T_a = 950 °C using Eq. (1): a) versus annealing time in a 500 nm-thick 1D crystal; and 2) versus the 1D nanocrystal size d after one hour annealing.

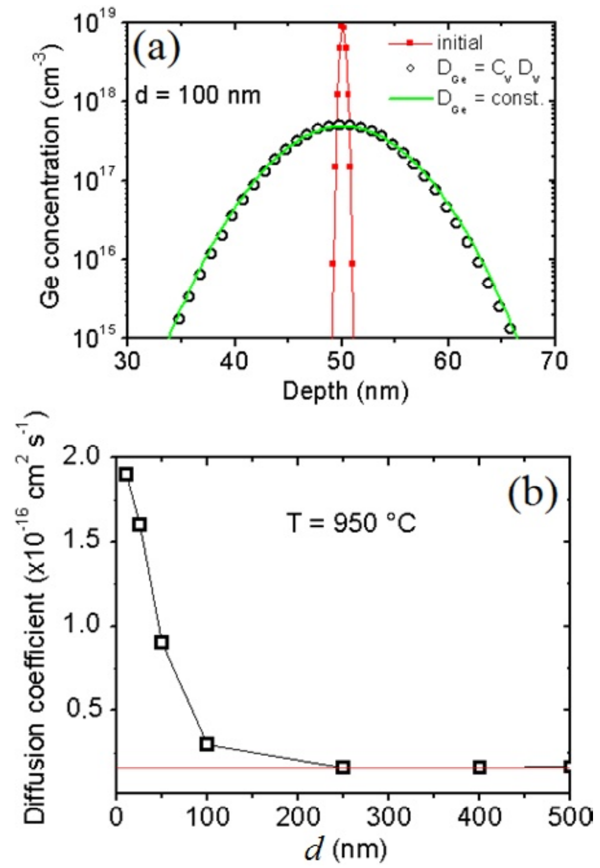

Fig. 3. Simulation results of Ge diffusion in a 1D Si nanocrystal using Eqs. (1) and (2): a) Ge concentration profiles in a 100 nm-thick 1D crystal, the red solid squares, the open solid circles, and the green solid line correspond to the initial Ge profile, the Ge profile after annealing at 950 °C for one hour, and the numerical fit of the Ge profile after diffusion using Eq. (3), respectively; b) variations of the Ge effective diffusion coefficient versus the nanocrystal size d.

attained, while $C_V^*(T_a)$ would need more time to be reached, depending on D_V and k. k is the only unknown parameter in Eq. (1), since D_V can be obtained from the literature. We choose to use the value from the same ref. [1] as for C_V^*, giving $D_V = 1 \times 10^{-9}$ cm^2 s^{-1} at T_a = 950 °C. k was determined simulating the vacancy concentration variations in an semi-infinite Si substrate during annealing at 950 °C using Eq. (1), and assuming that the depth of the vacancy concentration gradient from the surface to the bulk was smaller than 100 nm. Fig. 2a presents the vacancy concentration profile obtained for the same simulations performed in the case of a thin film exhibiting a thickness of 500 nm, for three different annealing time t = 1, 10, and 100 hours. The gradient profile observed close to the surface is identical to the one obtained in case of a semi-infinite substrate. It varies from $C_{Vs}^*(950\ °C) = 1 \times 10^{16}$ cm^{-3} and $C_V^*(950\ °C) = 8 \times 10^{14}$ cm^{-3}, and corresponds to $k = 5 \times 10^2$ s^{-1}. This profile is quickly obtained during the simulation, and thus, does not vary for the three annealing times investigated. Considering the same simulation parameters C_V^*, C_{Vs}^*, D_V, and k determined for T_a = 950 °C, one can perform the same simulation varying the thickness of the film. Fig. 2b presents the vacancy concentration profile obtained in layers exhibiting four different thicknesses d = 500, 100, 50, and 25 nm. One can note that due to the difference between the equilibrium vacancy concentration at the surface and in the bulk, and due to the kinetic parameters involved in simulation, the global vacancy concentration in the Si film increases when the thickness of the film decreases for thicknesses smaller than 100 nm. Assuming that Ge diffusion is mediated by the direct vacancy mechanism (no GeV pairs), the diffusion of a Ge Gaussian distribution located in the center of the film was simulated at T_a = 950 °C using the following equation

$$\frac{dC_{Ge}}{dt} = \frac{C_V D_V}{C_0} \frac{d^2 C_{Ge}}{dx^2}, \quad (2)$$

as well as using Eq. (1) describing vacancy concentration variations. $C_0 = 5 \times 10^{22}$ cm^{-3} is the Si atomic density. The simulation was performed for seven different film thicknesses d = 500, 400, 250, 100, 50, 25, and 10 nm. Fig. 3a presents the initial Ge distribution (red solid squares) located in the center of the film in the case of a 100 nm-thick film, as well as the diffusion profile (open circles) obtained after the simulation of one hour annealing. In order to extract an effective Ge diffusion coefficient (D_{Ge}), the obtained diffusion profiles were fitted using the Fick diffusion equation (green solid line in Fig. 3a):

$$\frac{dC_{Ge}}{dt} = D_{Ge} \frac{d^2 C_{Ge}}{dx^2}. \quad (3)$$

Fig. 3b presents D_{Ge}(950 °C) variations versus the film thickness (d). The solid red line corresponds to the equilibrium Ge lattice diffusion coefficient $D_{Ge}^* = C_V^* D_V / C_0$ = 1.6 × 10^{-17} cm^2 s^{-1} calculated using C_V^*(950 °C) = 8 × 10^{14} cm^{-3} and D_V(950 °C) = 1 × 10^{-9} cm^2 s^{-1} from ref. [1]. The Ge diffusion coefficient increases significantly when the film depth decreases below 100 nm. The Ge diffusion coefficient corresponding to the experimental nano-grains' average size (40 nm) in the nano-crystalline Si layer was taken from this figure and compared to the experimental diffusion coefficients in Fig. 4. In this last figure, the experimental Ge lattice diffusion coefficients measured in Si bulk by Hettich et al. [31] (dot line) and Dorner et al. [32] (dash line) are given versus temperature with the Ge diffusion coefficient measured in 40 nm-wide Si grains [14] (solid squares), and the simulated D_{Ge}(950 °C) (red open circle). D_{Ge}^* is also plotted (red solid circle). It is in quite good agreement with the experimental data from Hettich et al. and Dorner et al. Similar to the experiments, the simulated diffusion coefficient is found to be about one order of magnitude faster in the 40 nm-wide grains than in the bulk, due to an increase of vacancy concentration. Of course, the simulations are not quantitative since we only considered a single surface in a one-dimensional model (film geometry) instead of six interfaces in case of a cubic grain (3D geometry), and that k was not determined from experimental observations. However, these simple calculations show that an increase of the vacancy concentration may occur in some materials when the crystal size is reduced to tens of nanometers, depending on the difference of point defect concentration between the surface and the bulk, and depending on the point defect formation/annihilation kinetic in the considered material. One can also note that the density of extended defects such as dislocation is expected to be reduced in nanocrystals, and thus, point defect formation/annihilation kinetics should be different in nanocrystals and in macroscopic crystals.

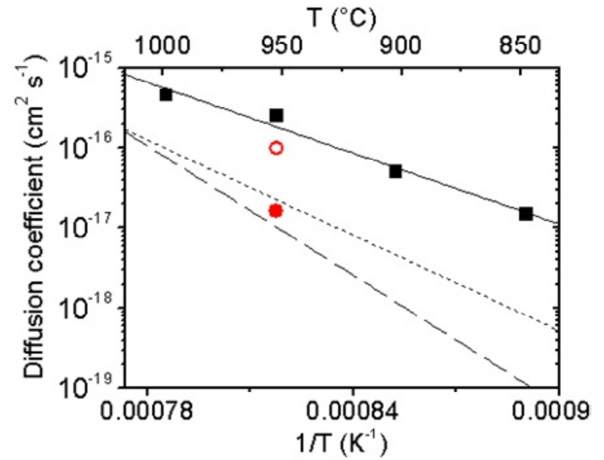

Fig. 4. Ge diffusion coefficients measured in the Si mono-crystal (dot line from [31] and dash line from [32]) and in 40 nm-wide Si grains (solid square [14]), compared with the corresponding coefficients obtained in the simulations at T = 950 °C (red solid circle in the mono-crystal and red open circle in the nano-grain).

4. CONCLUSION

APT measurements were performed on Si nano-crystalline layers, in which the Ge diffusion coefficient in the nano-grains was found to be faster than in macroscopic Si crystals. APT analyses did not evidence any extended defects in the nano-grains, nor grain boundary migration effects that could explain the faster diffusion of Ge atoms. All the Ge atoms detected by APT were found to be randomly distributed, and their 1D composition profiles were found to be in good agreement with the SIMS profiles used to measure the Ge diffusivity. Thus, considering that Ge diffusion in the Si nano-grains corresponds to Ge lattice diffusion, a possible explanation of the observed diffusion kinetic increase in nanocrystals is given, based i) on the difference of equilibrium vacancy concentration between the surface and the bulk of the nanocrystal, and ii) on point defect kinetics. Numerical simulations show that despite a significant difference in vacancy concentration between the surface and the bulk of a nanocrystal, an increase of vacancy concentration

in a nanocrystal is highly dependent on the diffusion coefficient and on the vacancy formation/annihilation rate in the material.

ACKNOWLEDGEMENTS

This work was supported by the French National Agency for Research (ANR) through the Program “Science de l’ingénierie” (Project DoGeTec, no. ANR-12-JS09-0015-1).

REFERENCES

[1] H. Bracht, N.A. Stolwijk and H. Mehrer // *Phys. Rev. B* **52** (1995) 16542.

[2] H. Bracht, J. Fage Pedersen, N. Zangenberg, A. Nylandsted Larsen, E.E. Haller, G. Lulli and M. Posselt // *Phys. Rev. Lett.* **91** (2003) 245502.

[3] V.V. Voronkov and R. Falster // *Mat. Sci. Eng. B* **134** (2006) 227.

[4] N.A. Stolwijk and H. Bracht, In: *Landolt-Bornstein-Numerical Data and Functional Relationships in Science and Technology*, ed. by D. Beke (Springer-Verlag, Berlin, 1998), Vol. III-33A.

[5] P. Pichler, *Intrinsic Point Defects, Impurities, and Their Diffusion in Silicon* (Springer-Verlag/ Wien, 2004).

[6] H. Mehrer, *Diffusion in Solids* (Springer-Verlag, Berlin Heidelberg, 2007).

[7] N.E.B. Cowerna, G. Manninoa, P.A. Stolka, F. Roozebooma, H.G.A. Huizinga, J.G.M. van Berkuma, F. Cristianob, A. Claverieb and M. Jaraíz // *Mat. Sci. Semicond. Process.* **2** (1999) 369.

[8] E. Lampin, V. Senez and A. Claverie // *Mat. Sci. Eng. B* **71** (2000) 155.

[9] A. Claverie, B. Colombeau, G. Ben Assayag, C. Bonafos, F. Cristiano, M. Omri and B. de Mauduit // *Mat. Sci. Semicon. Process.* **3** (2000) 269.

[10] F. Cristiano, J. Grisolia, B. Colombeau, M. Omri, B. de Mauduit and A. Claverie // *J. Appl. Phys.* **87** (2000) 8420.

[11] E. Lampina, F. Cristiano, Y. Lamrani and D. Connetable // *Mat. Sci. Eng. B* **124–125** (2005) 397.

[12] Y. Amouyal, S.V. Divinski, Y. Estrin and E. Rabkin // *Acta Mater.* **55** (2007) 5968

[13] A. Portavoce, G. Chai, L. Chow and J. Bernardini // *J. Appl. Phys.* **104** (2008) 104910.

[14] A. Portavoce, L. Chow and J. Bernardini // *Appl. Phys. Lett.* **96** (2010) 214102.

[15] M.R. Chellali, Z. Balogh and G. Schmitz // *Scripta Mater.* **65** (2011) 343.

[16] P. Stender, Z. Balogh and G. Schmitz // *Ultramicroscopy* **111** (2011) 524.

[17] H. Rösner, C. Kübel, Y. Ivanisenko, L. Kurmanaeva, S. V. Divinski, M. Peterlechner and G. Wilde // *Acta Mater.* **59** (2011) 7380.

[18] A. Portavoce, I. Blum, K. Hoummada, D. Mangelinck, L. Chow and J. Bernardini // *Defect and Diffusion Forum* **322** (2012) 129.

[19] M.R. Chellali, Z. Balogh and G. Schmitz // *Ultramicroscopy* **132** (2013) 164.

[20] D. Prokoshkina, L. Klinger, A. Moros, G. Wilde, E. Rabkin and S. V. Divinski // *Acta Mater.* **69** (2014) 314.

[21] A. Portavoce // *Scripta Mater.* **99** (2015) 37.

[22] C.-Y. Lin, Y.-K. Fang, S.-F. Chena, P.-C. Lin, C.-S. Lin, T.-H. Chou, J.S. Hwang and K.I. Lin // *Mat. Sci. Eng. B* **127** (2006) 251

[23] D. Irishika, K. Imamura and H Kobayashi // *Solar Energy Materials Solar Cells* **141** (2015) 1.

[24] A. Lyubchyk, S.A. Filonovich, T. Mateus, M.J. Mendes, A. Vicente, J.P. Leitão, B.P. Falcão, E. Fortunato, H. Águas and R. Martins // *Thin Solid Films* **591** (2015) 25.

[25] M. Zaborowski, P. Dumania, D. Tomaszewski, J. Czupryniak, T.Ossowski, M. Kokot, P. Paletko, T. Gotszalk and P. Grabiec // *Procedia Engineering* **47** (2012) 1053.

[26] R.A. Puglisi, C. Garozzo, C. Bongiorno, S. Di Franco, M. Italia, G. Mannino, S. Scalese and A. La Magna // *Solar Energy Materials Solar Cells* **132** (2015) 118.

[27] B. Xu, C. Li, M. Myronov, K. Fobelets // Solid-State Electronics **83** (2013) 107.

[28] R.A. Puglisi, S. Lombardo, G. Ammendola, G. Nicotra and C. Gerardi // *Mat. Sci. Eng. C* **23** (2003) 1047.

[29] E. Sun, F.-H. Su, C.-H. Chen and M.-J. Chen // *Appl. Surf. Sci.* **256** (2010) 5021.

[30] J.-N. Aqua, I. Berbezier, L. Favre, T. Frisch and A. Ronda // *Physics Reports* **522** (2013) 59.

[31] G. Hettich, H. Mehrer and K. Maier // *Inst. Phys. Conf. Ser.* **46** (1979) 500.

[32] P. Dorner, W. Gust, B. Predel, U. Roll, A. Lodding and H. Odelius // *Philos. Mag. A* **49** (1984) 557.

[33] A. Portavoce, K. Hoummada, A. Ronda, D. Mangelinck and I. Berbezier // *Beilstein J. Nanotechnol.* **5** (2014) 2374.
[34] A. Portavoce // *Scripta Mater*. **99** (2015) 37.
[35] A. Ishizaka and T. Doi // *Philos. Mag. Lett.* **65** (1992) 95.
[36] A. Natori and H. Harada // *Surf. Sci*. **438** (1999) 162.
[37] A. Portavoce, P. Gas, I. Berbezier, A. Ronda, J.S. Christensen, A. Yu. Kuznetsov and B. G. Svensson // *Phys. Rev. B* **69** (2004) 155415.
[38] A. Portavoce, I. Berbezier, P. Gas and A. Ronda // *Phys. Rev. B* **69** (2004) 155414.
[39] P. Asoka-Kumar, H.-J. Gossmann, F.C. Unterwald, L.C. Feldman, T.C. Leung, H.L. Au, V. Talyanski, B. Nielsen and K.G. Lynn // *Phys. Rev. B* **48** (1993) 5345.
[40] J. Oila, J. Kivioja, V. Ranki, K. Saarinen, D.C. Look, R.J. Molnar, S.S. Park, S.K. Lee and J.Y. Han // Appl. Phys. Lett. **82** (2003) 3433.